Available online at www.sciencedirect.com
ScienceDirect
International Journal of Heat and Mass Transfer 51 (2008) 3275–3286
International Journal of HEAT and MASS TRANSFER
www.elsevier.com/locate/ijhmt

Vortex formation and heat transfer in turbulent flow past a transverse cavity with inclined frontal and rear walls

A.Yu. D'yachenko, V.I. Terekhov *, N.I. Yarygina

Kutateladze Institute of Thermophysics SB RAS, 1, Acad. Lavrent'ev Avenue, 630090 Novosibirsk, Russia

Received 28 September 2007
Available online 31 January 2008

Abstract

The process of vortex formation, distributions of pressure coefficients, and convective heat transfer in a turbulent flow past a cavity with a low aspect ratio and inclined frontal and rear walls were experimentally studied. The angle of wall inclination φ was varied in the interval from 30° to 90°. Visualization techniques were applied to trace the evolution of the flow with the angle φ as the transverse cavity became more open. Pressure fields in the longitudinal and transverse sections on the bottom wall of the cavity, and on its frontal and rear walls, were measured. The measured distributions of temperature in the longitudinal and transverse sections on the three heated walls, and the obtained thermographic fields over the whole heated surface, were used to calculate local and average heat-transfer coefficients. It is found that in the interval of wall inclination angles $\varphi = 60$–$70°$ the flow in the cavity becomes unstable, with the primary vortex changing its structure from single-cellular to double-cellular. As a result, the distributions of static pressure and surface temperature across and along the cavity suffer dramatic changes. At smallest angles φ the flow re-attachment point gets displaced into the cavity to cause an abrupt growth of pressure and heat-transfer coefficients on the rear wall, which leads to a slight increase of the surface-mean pressure and heat transfer inside the cavity. At the angle of instability, $\varphi = 60°$, the local heat-transfer coefficient decreases markedly over the cavity span from the end faces of the cavity toward its center, and a most pronounced intensification of heat transfer is observed.

1. Introduction

In recent years, many studies of separated flows past various obstacles have been reported, such flows having numerous technical applications. Some of these studies were performed to examine flows past cavities. Trenches and cavities, intentional or incidental, are encountered on various aerodynamic surfaces. Among such surfaces are spacecraft hulls, gas-turbine channels, and surfaces with ribbing in heat exchangers and microelectronic chips. The shape of cavities used in power-engineering equipment ranges vastly. Yet, in the majority of theoretical and experimental studies of separated flows past transverse cavities, square- or rectangular-profiled cavities were examined [1–12]. Primary attention was paid to flow dynamics. Thermal characteristics remained less studied, although their accurate prediction is necessary for optimization of power plants and for further development of numerical methods in modeling turbulent separated flows in cavities.

The structure of the separated flow in a cavity is strongly affected by the ratio between the cavity height H and the cavity width L. Depending on the particular value of H/L, various flow regimes can be observed, having their own specific features in the case of square trenches, deep hollows, and shallow recesses (respectively, the cases of $H/L = 1$, $H/L \geqslant 2$, and $H/L \leqslant 0.1$). On passing from one to another regime, the shape, the position, and the total number of primary vortices inside the cavity undergo variation. For instance, the flow in a square trench gives an example of an eddy flow with closed streamlines.

Another important characteristic that affects the flow structure in a transverse cavity is the aspect ratio between the trench span and the trench width $s = S/L$. This ratio defines the type, either three- or two-dimensional, of the

* Corresponding author. Tel.: +7 383 3306736; fax: +7 383 3308480.
E-mail addresses: terekhov@itp.nsc.ru (V.I. Terekhov), yarygina@itp.nsc.ru (N.I. Yarygina).

0017-9310/$ - see front matter © 2008 Elsevier Ltd. All rights reserved.
doi:10.1016/j.ijheatmasstransfer.2007.11.039

Nomenclature

C_p	pressure coefficient, $2(p_i - p_0)/\rho U^2$
H	depth of cavity (mm)
L	width of cavity in the main flow direction (mm)
p	static pressure (N/m^2)
q	local wall heat flux (W/m^2)
Re_H, Re_L	Reynolds number ($U \cdot H/v$; $U \cdot L/v$)
S	length of cavity in the spanwise direction (mm)
Tu_0	free stream turbulence intensity ($\sqrt{\overline{u'^2}}/U$)
U	main flow velocity (m/s)

Greek symbols

α	heat-transfer coefficient (W/(m^2 K))
ρ	density (kg/m^3)
φ	inclination angle of cavity sidewalls
v	kinematic viscosity (m^2/s)

Subscripts

o	free-stream value in front of cavity
w	wall parameter

flow that develops in the cavity. The presence of three-dimensional vortical structures in transverse cavities with $S/L < 10$ was confirmed by numerous experimental data [4,5,8]. The formation of such structures in low-aspect-ratio cavities is explained, for the most part, by the accelerating action exerted on the flow by the end faces of the cavity, the flow in the case of $S/L > 10$ being purely two-dimensional. Here, three-dimensionality of the primary vortex is meant. The authors of [7] argue that, generally, the cavity flow involves both global and local three-dimensional formations. Three-dimensional pattern of the main flow is manifested in shear stresses developing on the end faces of the cavity and causing there a local reduction of the mean kinetic energy, thus making the flow more stagnant. That is why the flow pattern in the streamwise plane of symmetry (or in any other streamwise plane) is defined by the distance to the nearest end face of the cavity in combination with S/L.

The soot-oil visualization tests performed in [4] showed that the vortical structure in a cavity emerges as a succession of cells, each cell being a mirror reflection of the previous one, with a three-dimensional vortex formation pattern inherent to the flow in each cell. There are two possible configurations for different groups of cells, symmetric and asymmetric. Depending on the particular value of S/L, these structures can be symmetric or asymmetric, and the flow structure, all other conditions being identical, depends on the trench depth [5]. Based on their analysis of experimental data, the authors of [4] have drawn a conclusion that three-dimensional cellular structures are observed in cavities with $0.4 < H/L < 0.9$, the flow in square trenches being two-dimensional. This conclusion is not self-evident. It was shown in [8] that a symmetric cellular structure forms in cavities with $S/L = 2$, 4, 6, or 8, the number of the cells being half the value of the aspect ratio. In cavities with $S/L = 3$, 5, or 7, an asymmetric cellular structure is observed, with one of the extreme cells looking as an "incompletely" formed cell. In [8], the presence of a tornado-shaped motion at the interface between the primary vortex and the upstream secondary vortex, and mass ejection at the inter-cell boundary, were noted. It follows from the model proposed in [5] and developed in [8] that the shear layer that enters the cavity due to flow instability at the flow re-attachment point transforms in a tornado-shaped motion at the interface between two cells.

In several studies, local near-wall three-dimensional vortical structures developing in the flow past a rectangular cavity were examined. It was found in [6] that in the case of laminar flow in the upstream region of a cavity with $S/L = 1$, 2, or 3 (Reynolds numbers $Re < 10^4$), in between the cavity walls and the primary vortex, there develop ordered three-dimensional structures closely resembling Taylor–Gertler vortices. At higher Reynolds numbers, $Re > 10^4$, these vortices were found to break down. The authors of [7], who examined the behavior of the secondary vortex at the rear wall in cavities geometrically similar to cavities studied in [6], have attributed this phenomenon to turbulent pulsations produced in the boundary layer. The energy due to these pulsations was found to increase by more than tenfold compared to the case of laminar flow. Taylor–Gertler vortices are local three-dimensional structures that develop due to streamline bending in separated flows.

Heat-transfer studies performed for rectangular cavities with various proportions between the width and height were reported in [3,8,13–19,21–28]. In [3,8,22–28], the length of the transverse cavity L was a variable parameter, and the Reynolds number was calculated as $Re_L = UL/v$, where U is the free-stream velocity and v is the kinematic viscosity. In [17], the variable parameter was the trench height H, and, as the governing Reynolds number, the quantity $Re_H = UH/v$ was adopted. In extended rectangular cavities ($L/H \geqslant 2$) the primary vortex occupies part of the cavity, the shear layer not affecting noticeably the heat transfer. At fixed approach-flow conditions, the mean Nusselt number $\langle Nu_L \rangle = \langle \alpha \rangle L/\lambda$ is almost independent of the trench width, decreasing appreciably with increasing trench depth. The correlation dependence $\langle Nu_H \rangle = \langle \alpha \rangle H/\lambda = f(Re_H)$ does not depend on the parameter H/L. Here, the flow in a shallow transverse cavity in the cases of $Re_H < 5 \times 10^4$ and $Re_H > 5 \times 10^4$ displays, respectively the dependence for laminar boundary layer $\langle Nu_H \rangle \sim$

$Re_H^{0.5}$ and the dependence for turbulent boundary layer $\langle Nu_H \rangle \sim Re_H^{0.8}$, whereas in a deep cavity ($H/L > 1$) the main transfer mechanism is turbulent diffusion with $\langle Nu_H \rangle \sim Re_H^{2/3}$.

The question of how the three-dimensional structures affect the distribution of pressure and heat-transfer coefficients over the cavity span was most fully examined in [8], where measurements over the span of a cavity with $S/L = 8$ and $H/L = 0.66$, in which a symmetric regular cellular structure formed, were reported. The established nonuniformity of the static-pressure and temperature fields complied with the gas-dynamic structure of the flow.

It is of interest to dwell also on the study reported in [25], in which integral transfer of mass out of differently shaped cavities at axisymmetric expansion, including those with rectangular, semicircular, lenticular and other cross-sections was considered. The main drawn conclusion was that the transfer of mass weakly depends on the cavity shape provided that the Reynolds number is calculated from the mean flow velocity over the largest cross-section.

Nonetheless, to date the structure of three-dimensional flows in cavities largely remains obscure, few data being available on dynamic and thermal characteristics in low-aspect-ratio transverse cavities. In spite of the fact that the main contribution to the surface-mean heat transfer is made by the rear wall, in the majority of heat-transfer studies only the trench bottom was heated. It seems to be of interest to extend the heat-transfer studies to other thermal and geometric conditions. The latter is especially the case with cavities having inclined frontal and rear walls and presenting, in a way, analogues to transverse hemispherical flutes [12]. In the latter objects, a trade-off can be achieved between enhanced heat transfer and less pronounced increase in hydraulic resistance. The inclined rear wall provides for weaker pressure pulsations and lower amplitude of hydrodynamic oscillations in the flow re-attachment region. Apparently, these effects must influence the flow instability and vortex formation pattern and, hence, heat transfer.

In this work, we present data concerning the near-wall flow structure, distributions of pressure coefficients, and thermal characteristics for the flow past low-aspect-ratio cavities with inclined walls, whose inclination angle φ was varied in the interval from 30° to 90°.

In our previous studies [26,27] we showed that an increase in the angle of wall inclination from 45° to 90° has a profound effect on heat transfer. At $\varphi = 60°$ (here, as previously, φ is the angle between the trench sidewall and the trench bottom wall), enhanced heat transfer from the trench bottom is observed, whereas at $\varphi = 45°$, a delayed transition from laminar to turbulent heat transfer. Yet, in [26,27] only the trench bottom was heated, and heat-transfer measurements were made only in the midsection of the cavity. The present study covers a broader range of angles φ and, in addition, extends the investigations to the case with heated sidewalls. Next, the thermographic technique was employed to measure the rate of heat transfer over the whole heated surface.

2. Experimental equipment and parameters

The experiments were carried out in the wind-tunnel facility of the Institute of Thermophysics SD RAS. The test channel had cross-sectional dimensions 200 × 200 mm, the length being 1000 mm. On the channel bottom, a model with a trench was installed, placed in between two flat aerodynamic panels. Upstream of the trench, the length of either panel was 480 mm, the length of the downstream portion being 200 mm. We examined the flow past a cavity whose dimensions were as follows (see Fig. 1): depth $H =$ 60 mm, width at the bottom $L = 60$ mm, and length in the crossflow direction $S = 180$ mm. So, we had a low-aspect-ratio cavity with $S/H = 3$ and $H/L = 1$. All in all, six models were employed in tests, intended for soot-oil and thermographic visualization tests and for measurements of pressure fields and fields of thermal characteristics. In the model intended for heat-transfer measurements to be performed with the help of thermocouples, the trench walls were prepared from 20-mm thick textolite sheet. The experiments were carried out at wall inclination angles $\varphi = 30°$, 45°, 60°, 70°, 80°, and 90°. The angle φ was varies so that to keep the trench height H and the trench length L (in the direction of the flow) unchanged. The sidewall length L_w varied according to the angle φ.

The measurements were performed in the range of free-stream velocities $U = 5 \div 35$ m/s, these velocity values yielding Reynolds numbers $Re_H = HU/\nu = 2 \times 10^4 \div 1.4 \times 10^5$. At all flow velocities, the boundary layer upstream of the cavity was turbulent. The boundary-layer momentum thickness prior to flow separation, $\delta^{**} = \int_0^{\delta} \frac{\rho U}{\rho_0 U_0} \cdot \left(1 - \frac{U}{U_0}\right) \cdot dy$, calculated from the experimental profiles of flow velocity, varied, according to the Reynolds number, in the interval from 3.2 to 3.7 mm, yielding for the boundary-layer thickness a value of $\delta \approx 35$ mm. The turbulence number in the approaching channel flow, measured with the help of a DISA-55M hot-wire anemometer, was 1.5%.

It was believed for a long time that the flow inside a trench is always turbulent because near the flow separation point there develops a Kelvin–Helmholtz instability making the shear-layer flow turbulent. The turbulent flow, however, is laminarized in the recirculation region as the stream, under the action of a favorable pressure gradient,

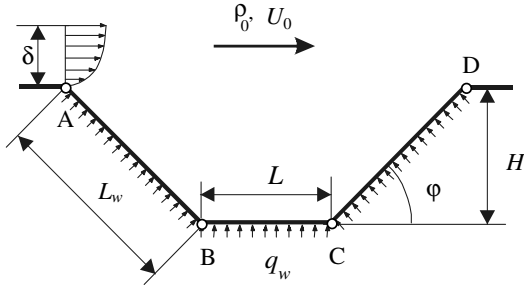

Fig. 1. The flow past the cavity.

turns around behind the flow re-attachment point. The authors of [16,17], who examined the mean heat-transfer coefficients in a transverse trench under conditions of laminar and turbulent flow, pointed to the presence of a laminar-turbulent transition. In [18], studies were carried out for a rectangular trench with the above-indicated geometric parameters, both for laminar and turbulent flow conditions. The transition was shown to occur at $Re_H = 4.3 \times 10^4$. Based on this value, it can be concluded that in the present experiments in the indicated range of Reynolds numbers the flow in the trench was turbulent.

Special attention was paid to guarantee that the cavity was aligned normally to the flow since detailed studies showed that the flow in a rectangular cavity is unstable with respect to slightest trench misorientation. Small angular deviations (within 1°) from the direction normal to the flow violate the flow symmetry in the cavity.

In measuring the distribution of static pressure in the cavity, the model was provided with 80 pressure taps, 0.5 mm in diameter, located on the frontal and rear walls, and also on the bottom of the cavity, in six sections, two sections being located on each of the three walls.

A strip heater prepared from 0.36-μm thick and 5-mm wide aluminum foil, with 0.5-mm winding separation, was used to heat the walls and the bottom of the cavity in the regime with constant heat-flux density. The trench surfaces were supplied with 158 chromel–copel thermocouples arranged in three longitudinal sections on the bottom wall, five longitudinal sections on the sidewalls, and in four sections across the flow (one section on either sidewall and two sections on the bottom wall). To estimate the heat leaks through the plate, four thermocouples were calked into the backside of each heated wall.

In the thermographic tests, the cavity provided with the heater was flush-mounted on a wind-tunnel channel sidewall. The cavity was heated during one hour in a necessary heating mode and, then, the wall temperature was subsequently measured with a THERMO TRACER TH7102 IR imager (Japan). The experimental thermographic procedure was described in detail elsewhere [29]. Surface scans were made to grasp a 192 × 192 pixel frame. The obtained temperature field was digitized using readings of at least two thermocouples; afterwards, a special computer code was used to construct the thermograms.

To diminish parasitic heat overflows, the thermal models were provided with thermal insulation. The relative error in measuring the heat-transfer coefficients estimated with due allowance for convective and emissive heat transfer was within 7–11%.

3. Experimental results and discussion

3.1. Flow visualization data

The oil-film technique was used to visualize the flow pattern in the cavity for various angles of inclination of the frontal and rear walls. The sidewalls and the end faces of the cavity in these tests were prepared from 10-mm thick turbonit, and the bottom wall was prepared from 5-mm thick plexiglass. To reveal the flow pattern, a mixture of lamp oil and offset black was applied, with a syringe, onto the trench walls. The visualization on the end faces was carried out on a cavity raised in the upright position. The pictures obtained were converted in electronic form using a scanner, and were subsequently processed on a computer.

Under stringent normal conditions, the vortex formation pattern in the cavity with $\varphi = 90°$ is symmetric, displaying one primary vortex (Fig. 2). For transverse cavities with all angles φ flow patterns in the vicinity of the bottom, frontal and rear walls were obtained, also shown in Fig. 2. These data were partially presented in [13,14,19]. With variation of φ, the visualized flow patterns vary appreciably. With decreasing inclination angle, the flow becomes more and more three-dimensional. It is also seen that at $\varphi = 90°$ the primary vortex resides at the center of the cavity, whereas at $\varphi = 80°$ this vortex is displaced closer to the rear wall. In both cases, the primary vortex appears as a single cell. As the cavity becomes more open, the shear-stress asymmetry becomes more pronounced, giving rise to elliptic-type instability (terminology of [20]). At angles $\varphi < 70°$ at the center of the cavity there arises an intense mass flow directed from the rear to frontal wall, and the primary vortex decomposes into two cells. The double-cellular structure is also observed in cavities with $\varphi = 30°$, 45°, and 60°. At $\varphi = 70°$, the vortex formation pattern is indistinct because of strong flow instability. In the case of cellular structure of the primary vortex, the role played by corner vortices becomes more significant, the primary vortex being pushed from the walls. Nucleation of a transverse mass flow at the rear wall can be distinctly traced, followed by its impact onto the frontal wall. At the end faces the vortex flow in the cavity becomes asymmetric, the center of the primary vortex being shifted closer to the frontal wall. The decomposition of the primary vortex into two vortices at $\varphi < 70°$ is registered in sidewall projections, both resultant vortices being pushed away from the end faces.

The alteration of flow modes from an unstable single vortex to a stable double-cellular structure also depends on the flow Reynolds number (see Fig. 3). The flow structure can be traced most distinctly at $Re_H = 8 \times 10^4$. Based on all performed tests, it was found that in the case of $Re_H = 4 \times 10^4$ the decomposition of the primary vortex into two vortices occurs at $\varphi \approx 60°$, and in the case of $Re_H = 1.2 \times 10^5$, at $\varphi \approx 80°$. At $\varphi = 70°$, with increasing number Re_H the flow of mass from the rear to frontal wall becomes less intense.

3.2. Thermographic visualization of the flow pattern

The IR imager was employed to perform thermographic visualization of the temperature field for various angles φ. This visualization has supplemented and refined the vortex-formation picture in the cavity. The model with heated

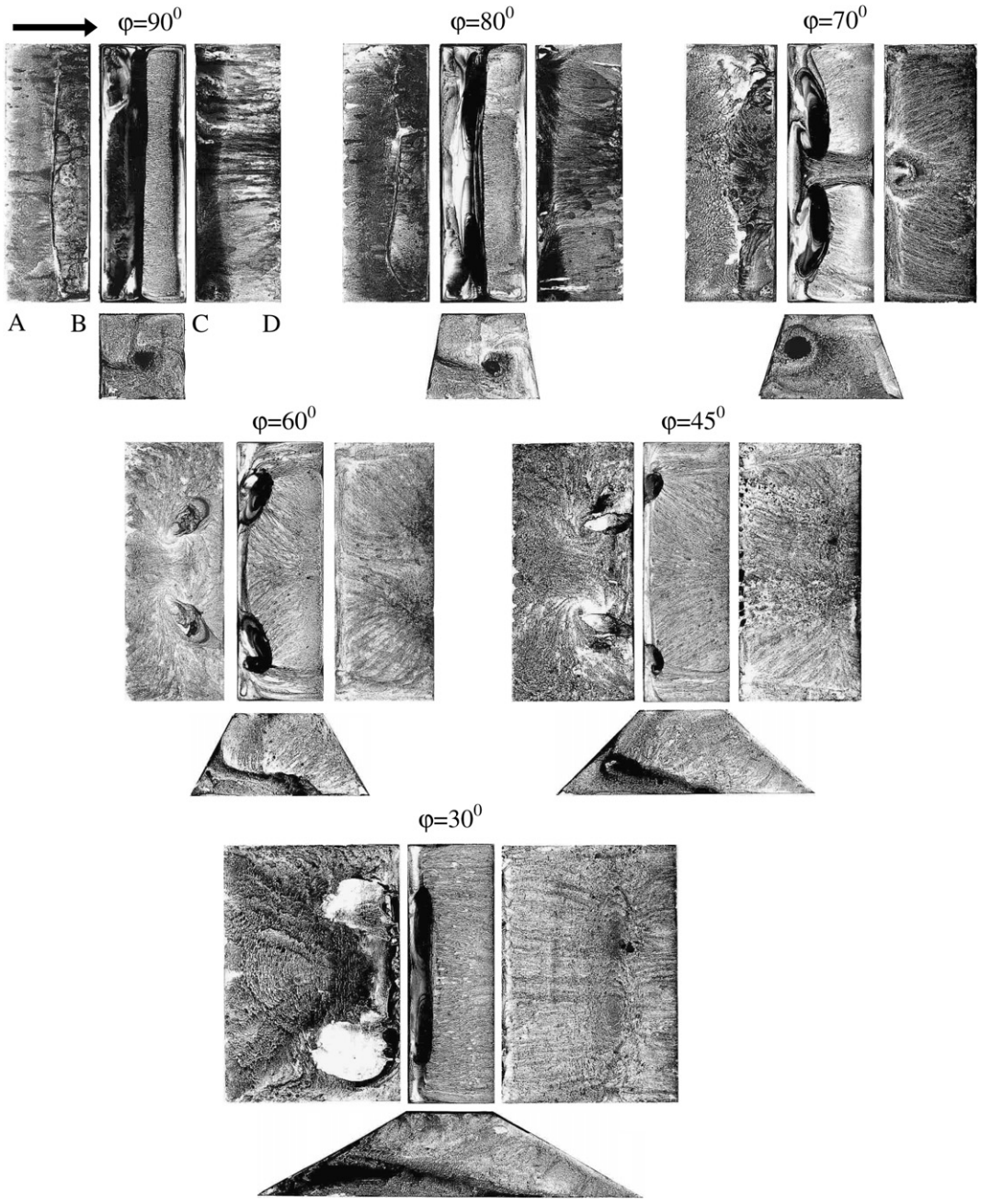

Fig. 2. Evolution of the vortex-formation pattern in the cavity with variation of the wall inclination angle ($Re_H = 8 \times 10^4$).

bottom and sidewalls was mounted, in upright position, on the sidewall of the wind-tunnel channel. Underneath the heater, chromel–copel thermocouples were provided, spaced 10 mm apart from each other over the cavity span and insulated from the heater by a heat-resistant varnish layer. The thermocouples were used to relate the thermal pictures obtained in the IR portion of the spectrum to real temperatures. The heating was carried out in the regime $q_w = \text{const}$. The heat loss through the bottom was estimated from the temperature difference across the bottom plate using several thermocouples installed on the lower surface of the plate. The distribution of temperature over the bottom wall for cavities with large angles of wall inclination is shown in Fig. 4. The isotherms in Fig. 4 were determined from the difference between the wall and flow temperatures. It can be concluded from the obtained thermograms that in the inclined cavity with $\varphi = 70°$ near the rear wall there arises a vortex flow with double-cellular structure. On the whole, the thermographic visualization data well comply with soot-oil visualization data, proving the cavity flow to be essentially three-dimensional. The temperature is maximal at the centers of the large-scale vertical cells. In the case of $\varphi = 70°$, with an instability arising in the flow, the center of the cell becomes blurred, the temperature being lower than that for other angles. In the case of small wall inclination angles, $\varphi = 30°$ and 45°,

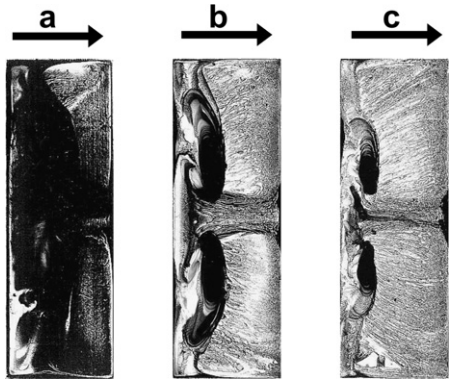

Fig. 3. Visualization data for the bottom flow in the cavity with $\varphi = 70°$: (a) $Re_H = 4 \times 10^4$; (b) $Re_H = 8 \times 10^4$ and (c) 1.2×10^5.

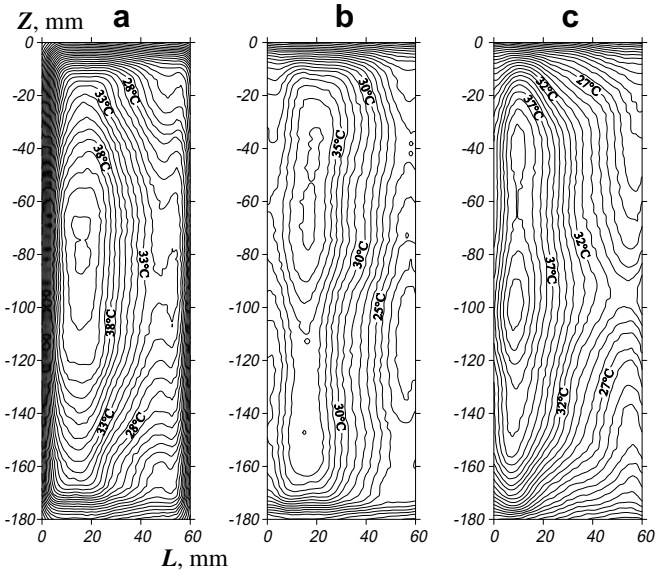

Fig. 4. Distribution of temperature over the cavity bottom at $Re_H = 8 \times 10^4$: (a) $\varphi = 90°$; (b) $\varphi = 80°$ and (c) $\varphi = 70°$.

the highest temperature is observed at the centers of the cells, which in this case reside closer to the frontal wall.

3.3. Distribution of pressure coefficients

A good correlation is observed between the obtained vortex-formation picture and the distribution of the pressure coefficient $C_p = 2(p_i - p_0)/(\rho U^2)$ over the bottom and sidewalls of the cavity (here, p_i is the wall pressure, and p_0 and U are the pressure and the flow velocity measured at a height of 100 mm from the surface of the model upstream of the cavity). The pressure coefficients were measured for all angles of wall inclination along the streamwise midsection of the bottom surface and the frontal and rear walls. Moreover, the distributions of pressure over the transverse midsection of the cavity bottom, and over transverse sections on the frontal and rear walls located at a distance of 40 mm from the cavity edges, were obtained.

A test distribution of pressure over the midsection of a square cavity is shown in Fig. 5. This distribution is compared with other reported data [31] obtained at roughly identical free-stream velocities. A fairly good agreement is observed.

A typical distribution of the pressure coefficient along the cavity is shown in Fig. 6. In the cases of $\varphi = 90°$, 80°, and 70°, the curves in Fig. 6 behave quite similarly, the value of C_p somewhat increasing with decreasing wall inclination angle. The highest pressure is observed on the frontal wall, falling in value on the bottom and rear walls, with rarefaction taking place over the greater part of the surface for the indicated angles. On approaching the exit cavity edge, the pressure rapidly increases. At the angle $\varphi = 60°$, when a double-cellular flow structure forms, the pressure starts decreasing. At $\varphi = 45°$ and 30° the pressure distribution suffers appreciable changes, exhibiting rarefaction on the frontal and bottom walls of the cavity and a profound rise at the rear wall. At $\varphi = 45°$ at the exit cavity edge the coefficient C_p is approximately twice its value at $\varphi = 90°$. In the case of $\varphi = 30°$ the flow re-attachment point is shifted into the cavity, with a pressure maximum observed near the exit edge.

The redistribution of pressure due to the vortex-formation processes is observed even more distinctly in transverse sections of the cavity (see Fig. 7). At $\varphi = 90°$, the pressure is quite uniform over the cavity span on all the three walls. In the case of $\varphi = 80°$ and, especially, $\varphi = 70°$ and 60°, with the suction of mass at the cavity center opposing the main flow, a strong asymmetry emerges in the distribution of pressure coefficients, with a maximum in the midsection and a considerable rarefaction near the butt-ends on the frontal wall and on the bottom. The formation of a double cellular vortex is most clearly manifested in the distribution of pressure in the cavity with $\varphi = 45°$: on the frontal wall and on the bottom, two minima at the centers of the cells are observed, with a sharp pressure rise exhibited near the end faces. The pressure increases especially strongly on the rear wall, with pressure maxima corresponding to the centers of the cells. At $\varphi = 30°$, the distribution of pressure over all walls is most uniform. The pressure on the rear wall is even more strongly increasing in comparison with $\varphi = 45°$. Thus, reconstruction of the cavity flow with decreasing wall inclination angle results in a profound redistribution of pressure coefficients. Estimates show that at $\varphi = 30°$ the surface-mean pressure coefficient is approximately 20% increased compared to the case of a rectangular cavity.

A most important characteristic of obstacles is their aerodynamic resistance. In the present study, no such measurements were performed because of their complexity; yet, an estimate of pressure losses can be obtained from the distributions of pressure measured on the sidewalls of the cavity. The loss of pressure in the cavity was estimated from experimental data as the sum of the projections of wall pressure forces onto the vertical axis y. The data on the integral pressure coefficients are presented in Fig. 8.

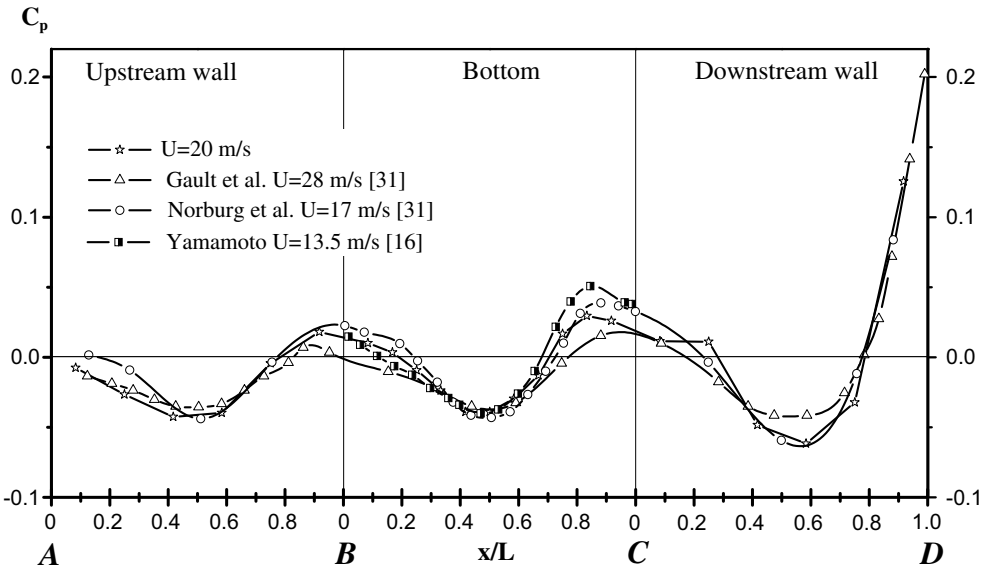

Fig. 5. Comparison of pressure coefficients in the midsection of a square cavity with the data reported by other authors at close flow velocities.

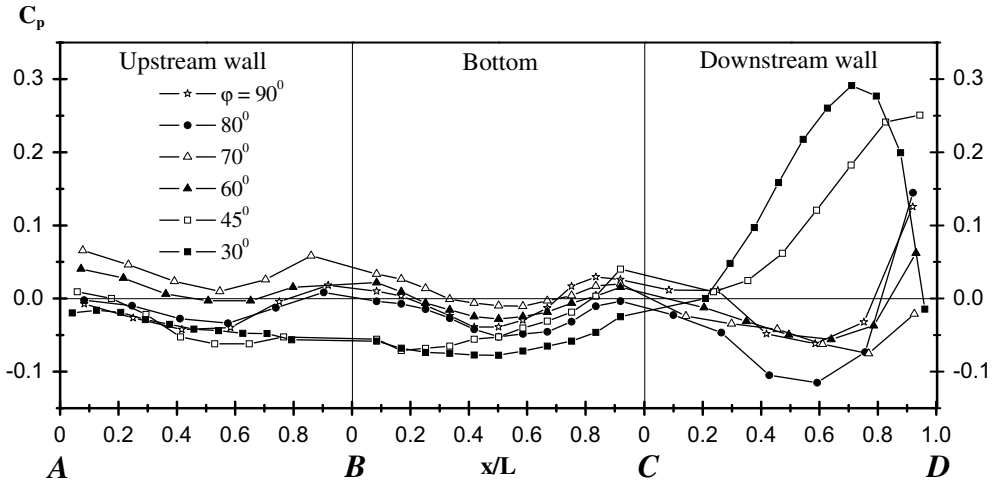

Fig. 6. The distribution of pressure in the midsection of the cavity.

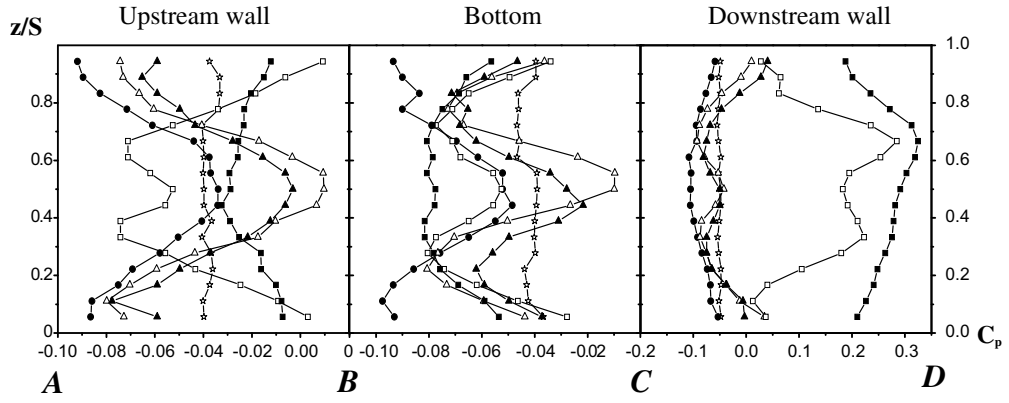

Fig. 7. The distribution of pressure over the cavity span (the designations are the same as in Fig. 6).

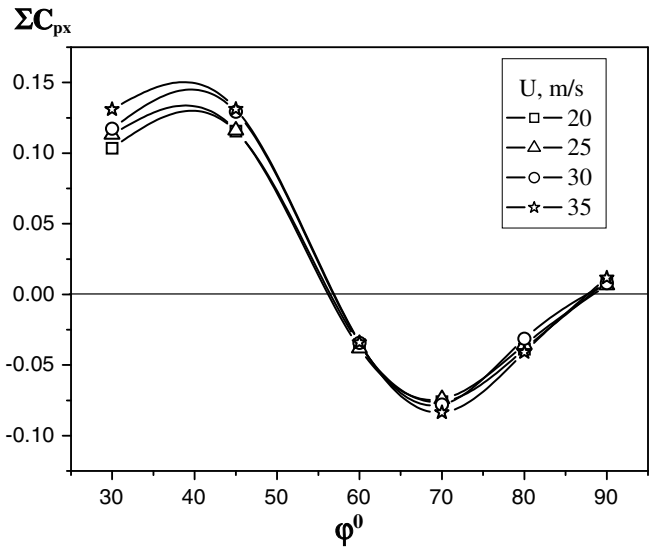

Fig. 8. The integral value of pressure coefficients on the frontal and rear walls.

Interestingly, a highest pressure is observed at small inclination angles; at $\varphi = 80$–$60°$ the pressure integral is negative, approaching zero at $\varphi = 90°$. It can be expected that the total aerodynamic pressure in the case of large angles would be also low compared to small angles. The latter can be attributed to the fact that in the case of open cavities with $\varphi < 60°$ a constantly increasing fraction of mass enters the cavity from the gas mixing layer.

3.4. Heat transfer

The thermocouple-probing and IR-imaging data were used to calculate the local heat-transfer coefficients

$$\alpha_i = (q_w - \Delta q)/(T_{wi} - T_0).$$

Here, q_w is the specific heat flux, Δq is the heat loss, T_0 is the free-stream temperature, and T_{wi} is the local wall temperature.

Typical distributions of the local heat-transfer coefficients α_i in the streamwise midsection on the frontal, rear, and bottom wall of the cavity for all the examined angles φ are shown in Fig. 9. Along the abscissa axis, the current coordinate on each wall, normalized to the wall length, is plotted. On the bottom wall the spread of experimental points for all angles of wall inclination is insignificant, with some intensification of heat transfer observed at $\varphi \leqslant 60°$, in which case the primary vortex decomposes into a double-cellular structure. At these angles, three-dimensionality of the cavity flow becomes more pronounced, and the vortex-formation process is similar to that observed in a hemispherical cavity [30]. On the frontal wall, a different effect of the angle φ on the rate of heat transfer is observed: at $\varphi = 45°$ and, to a greater extent, at $\varphi = 30°$ the heat-transfer intensity decreases sharply. On the rear wall, as the angle φ decreases, the heat-transfer coefficient increases markedly. On this wall, near the bottom at $\varphi = 30$ and $45°$ the value of α_i is 1.7 times greater than that at $\varphi = 90°$. According to the data of Fig. 9, it is the rear wall of the cavity where the highest heat-transfer intensity is reached, especially in the region adjacent to the rear cavity edge.

Fig. 10 shows heat-transfer coefficients averaged over the midsection length; the data are given for each of the walls at various free-stream velocities in cavities with various angles of wall inclination. Of course, the value of $\langle\alpha\rangle$ increases with increasing flow velocity. On the frontal wall the heat-transfer intensity is maximal at $\varphi = 60°$, i.e., at the moment at which the primary vortex in the cavity decomposes into two vortices. At the bottom and rear walls the heat-transfer rate decreases with increasing angle φ. A most pronounced reduction of the heat-transfer coefficient

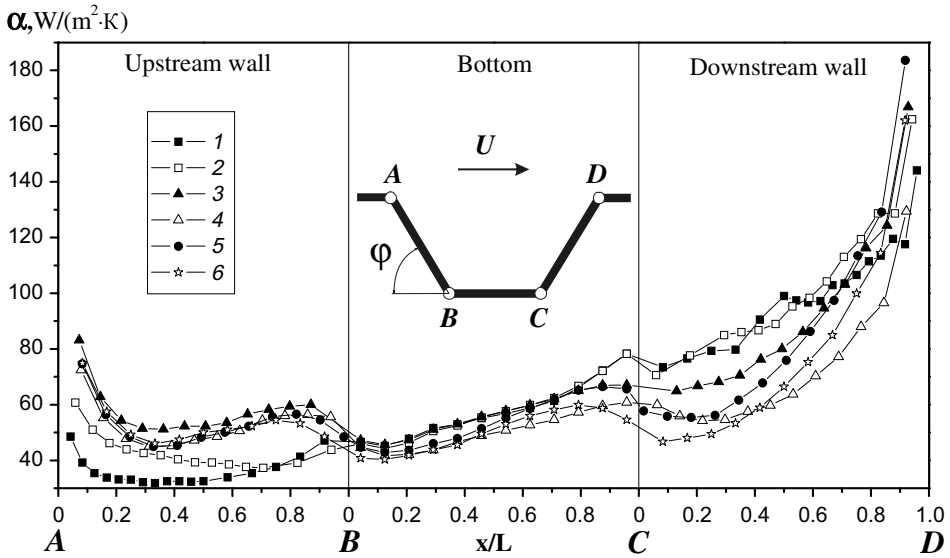

Fig. 9. The distribution of the local heat-transfer coefficient in the midsection of the cavity at $Re_H = 4 \times 10^4$: (1) $\varphi = 30°$; (2) $\varphi = 45°$; (3) $\varphi = 60°$; (4) $\varphi = 70°$; (5) $\varphi = 80°$; (6) $\varphi = 90°$.

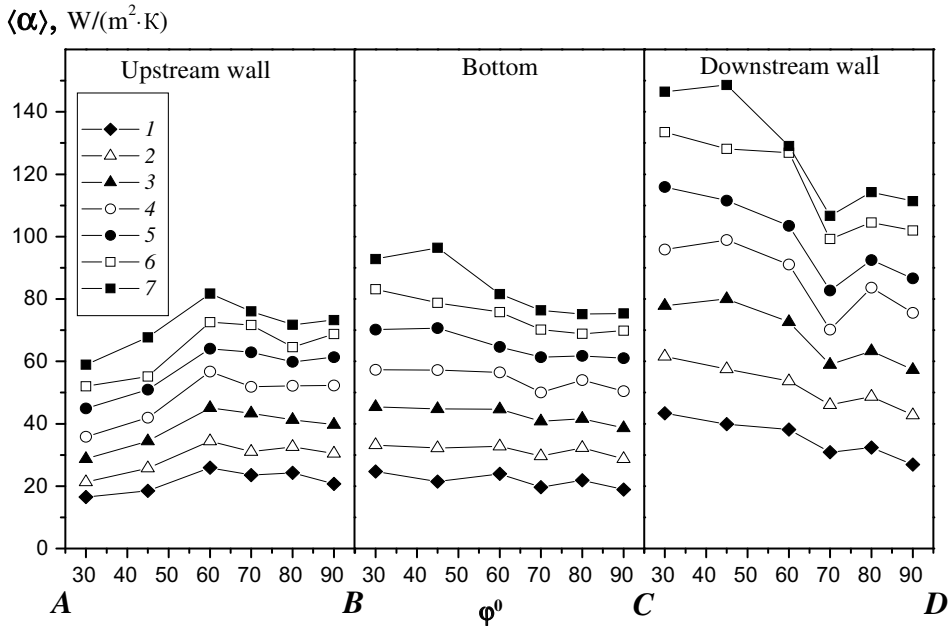

Fig. 10. The heat-transfer coefficient averaged over the midsection length versus the wall inclination angle φ: (1) $U = 5$ m/s; (2) $U = 10$ m/s; (3) $U = 15$ m/s; (4) $U = 20$ m/s; (5) $U = 25$ m/s; (6) $U = 30$ m/s; (7) $U = 35$ m/s.

is observed at $\varphi = 70°$, i.e., when, prior to reconstruction of the vertical structure, the cavity flow becomes extremely unstable. This behavior demonstrated by the heat-transfer coefficient can be attributed to the origination of the so-called elliptic instability induced by asymmetrically applied shear stresses [1]. The flow-instability effect is more pronounced at high free-stream velocities.

The cavity flow being three-dimensional, the midsectional distributions of α_i and $\langle\alpha\rangle$ do not give a comprehensive idea on heat transfer over the entire surface of the cavity. Fig. 11 shows the distributions of heat-transfer coefficients over the cavity span. On the frontal and rear walls the sections with thermocouples were provided at a distance of 35 mm from the upper edges, and on the bottom wall two such sections were provided at a distance of 15 mm from the frontal and rear walls. The general behavior demonstrated by the heat-transfer coefficient over the span of cavities with different angles φ (see Fig. 11) is consistent with the topological vortex-formation picture. On the frontal wall there exists a fairly extended region where heat transfer depends weakly on φ for $\varphi = 60$–$90°$. In the case of wide-open cavities with $\varphi = 30$–$45°$ the heat-transfer intensity decreases by a factor of 1.45, and remains roughly constant over the cavity span except for regions close to the end faces. On the bottom of the cavity with $\varphi = 70°$, during the origination of the counter-flow the heat-transfer coefficients sharply decrease over the cavity span from the end faces toward the center, where a minimum value of α is attained. It should be noted here that a similar behavior was also demonstrated by the pressure coefficient. A decrease of heat transfer toward the center was also observed in cavities with $\varphi = 60$ and 80°; yet, in the latter

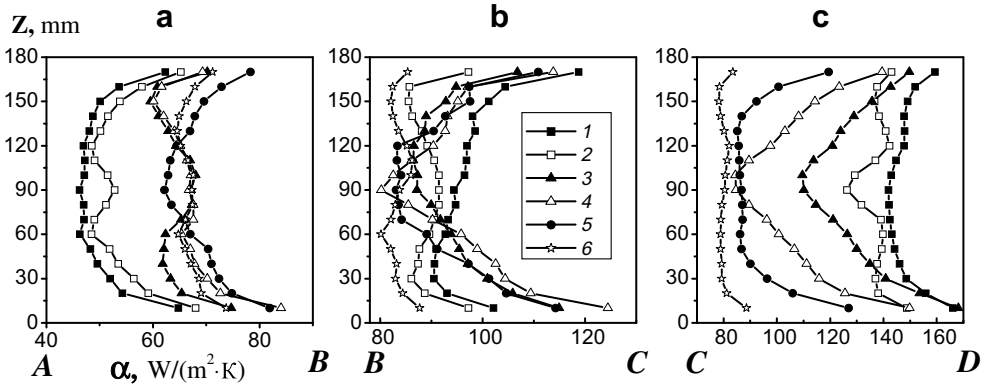

Fig. 11. The distribution of local heat-transfer coefficients over several spanwise sections of cavities with various angles φ at $U = 30$ m/s: (a) frontal wall; (b) bottom wall; and (c) rear wall; the designations are the same as in Fig. 1.

cases there were narrow central regions with roughly uniform heat-transfer coefficient. On the rear wall, no qualitative changes in the spanwise behavior of heat-transfer coefficients were observed. The heat-transfer coefficient increases markedly with increasing angle φ as the cavity becomes more opened.

The temperature fields obtained by thermography and thermocouple measurements were used to calculate the surface-mean heat-transfer coefficients and the corresponding Nusselt numbers Nu_H. The averaged data obtained with the two methods on the bottom of the cavity with $\varphi = 90°$ were found to well agree with each other. Yet, at larger angles φ the averaged thermographic data obtained on the frontal and rear walls were found to appreciably differ from the data obtained by thermocouple measurements. In this connection, graphs in Figs. 12–14 were plotted using thermocouple data measured in all sections.

Fig. 12 shows the Nusselt number $\langle Nu_H \rangle$ averaged over the entire heated surface versus the Reynolds number Re_H at various angles φ. The straight lines in Fig. 12 refer to formulas of [16] for laminar and turbulent laws of heat transfer in a rectangular cavity. For all angles φ, beginning from $Re_H = 4 \times 10^4$, the dependence $Nu_H \sim Re_H^{2/3}$ is valid, typical of separated flow with the diffusion transfer mechanism. In the case of wide-open cavities with $\varphi = 30$ and 45° and flow velocities $U = 5 \div 10$ m/s the heat transfer corresponds to laminar flow, being conditioned by flow features on the frontal wall. It is the laminar character of the flow at these angles that defines the reduction of the local heat-transfer coefficient on the frontal wall (see Fig. 9). The curves of Nusselt number averaged over the whole cavity surface versus the angle φ are shown in Fig. 13. Some increase in the mean heat-transfer coefficient at $\varphi \leqslant 60°$ can be noted, the largest value of $\langle Nu \rangle$ being observed at

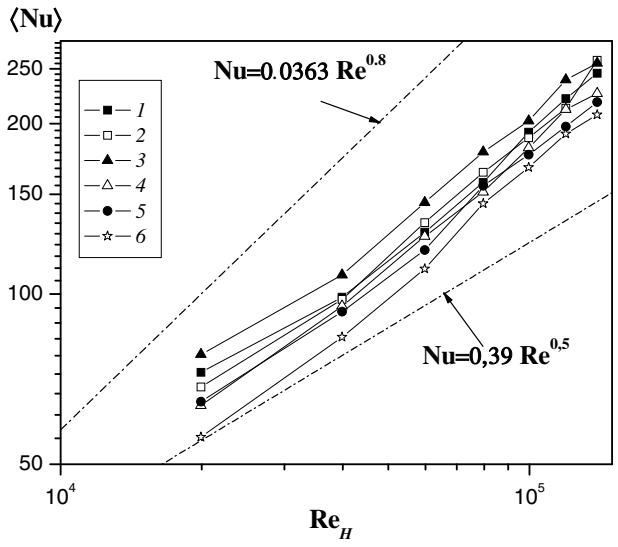

Fig. 12. The mean Nusselt number calculated over the entire heated surface versus the Reynolds number for various angles φ (the designations are the same as in Fig. 9) in comparison with the theoretically predicted curves [16].

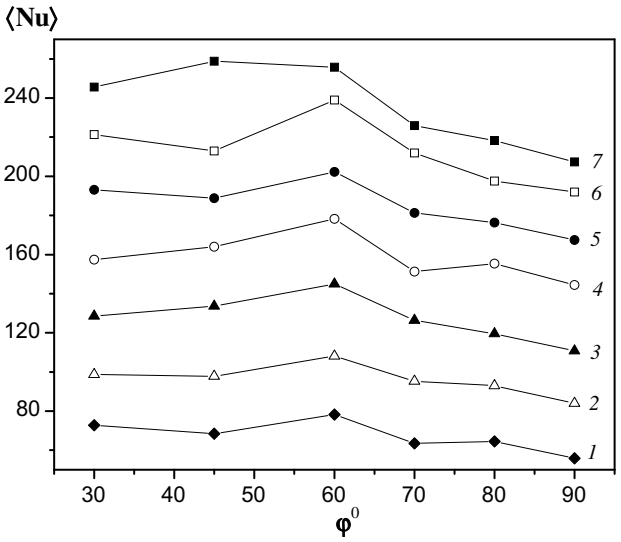

Fig. 13. The mean Nusselt number calculated over the entire heated surface versus the angle φ at various flow velocities (the designations are the same as in Fig. 10).

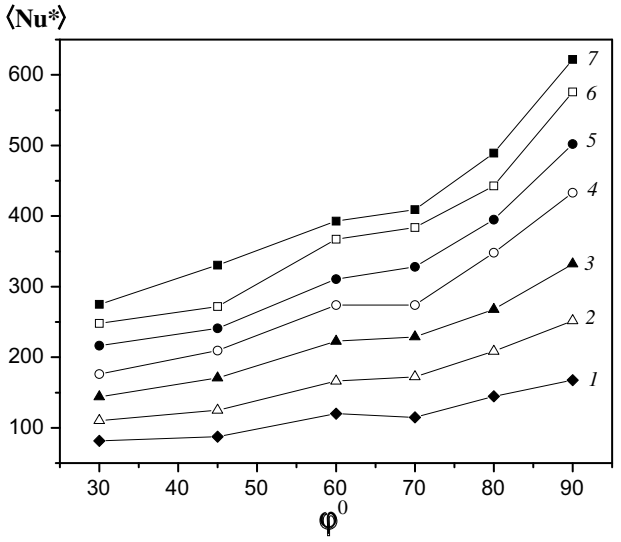

Fig. 14. The mean Nusselt number determined over the interface between the cavity and the external flow versus the angle φ at various flow velocities (the designations are the same as in Fig. 10).

$\varphi = 60°$, when the double-cellular structure emerges in the cavity flow. In fact, the dependence of the mean Nusselt number on the wall inclination angle is quite weak.

The net intensification of heat transfer in the cavity, however, is given by the mean value of $\langle \alpha \rangle$ calculated over the interface between the cavity and the external flow rather than by the mean heat-transfer coefficient averaged over the entire heated surface. Fig 14 shows the curve of the Nusselt number calculated over the interface between the cavity and the external flow versus the angle φ at various free-stream velocities. With decreasing angle φ, the latter interface grows in area to make the mean Nusselt number decreasing. Nonetheless, a non-monotonic behav-

ior of the curve $\langle Nu \rangle = f(\varphi)$ can be noted, resulting from some local heat-transfer intensification at $\varphi = 60°$ and an insignificant reduction of heat transfer at $\varphi = 70°$.

It can be added to the aforesaid that heat transfer behind a transverse cavity needs to be further investigated. In this case, by analogy with hemispherical cavities [30], heat-transfer intensification behind cavities with large opening angles in the downstream region one-caliber long can be expected to occur due to self-sustained oscillations that arise in the case of double-cellular vortex structure of the cavity flow. Another interesting problem is the action of high-level free-stream turbulence on the heat transfer in a cavity with inclined sidewalls. Some newly obtained data [28] are indicative of up to 40% heat-transfer enhancement in a cavity at a free-stream turbulence number of 15%, this value being well in excess of the heat-transfer enhancement behind a rib or a step.

4. Summary

An experimental study was performed to examine dynamic and thermal characteristics in a low-aspect-ratio transverse cavities ($S/H = 3$) with various inclination angles of the frontal and rear walls ($\varphi = 30°$, 45°, 60°, 70°, 80°, and 90°) in the range of Reynolds numbers $Re_H = 2 \times 10^4 \div 1.4 \times 10^5$.

The soot-oil and thermographic visualization data, and the measured pressure and temperature distributions, showed the flow in the cavity to be essentially three-dimensional. Depending on the flow Reynolds number, at $\varphi = 60°$ or 70° the vortex-formation pattern suffers dramatic changes owing to a developing instability. Instead of a single-cell vortical structure, a double-cell structure emerges. At small wall inclination angles, the flow structure largely affects the behavior of pressure coefficients. Estimates show the surface-mean pressure coefficients at $\varphi = 30°$ to be increased approximately by 20% in comparison with a rectangular trench.

Local coefficients of heat transfer on the three walls in the midsection and in several sections over the cavity span were measured. It is shown that, as the angle φ decreases, the heat-transfer coefficient at the rear wall increases markedly. During the reconstruction of the flow, observed at the angles $\varphi = 60°$, 70°, and during the origination of a counter-flow moving from the rear to frontal wall, the distribution of heat-transfer coefficients displays a sudden drop over the cavity span toward the center. On the emergence of instability in the cavity with $\varphi = 60°$, the heat-transfer coefficient averaged over the entire heated surface increases profoundly.

Acknowledgement

This work was partially supported by the Russian Foundation for Basic Research (Grant No. 06-08-00300).

References

[1] D. Rockwell, E. Naudascher, Review – self-sustaining oscillations of flow past cavities, Trans. ASME, J. Fluids Eng. 100 (2) (1978) 152–165.
[2] I.M. Varfolomeev, G.A. Glebov, Yu.F. Gortyshov, Structure and characteristics of a turbulent separated flow in a cavity, J. Eng. Phys. 48 (3) (1985) 387–391.
[3] R. Haugen, A. Dhanak, Heat transfer in turbulent boundary-layer separation over a surface cavity, Trans. ASME, J. Heat Transfer 89 (3) (1967) 335–342.
[4] D.J. Maull, L.F. East, Three-dimensional flow in cavities, J. Fluid Mech. 16 (4) (1963) 620–632.
[5] A.L. Kistler, F.C. Tan, Some properties of turbulent separated flows, Phys. Fluids Suppl. 10 (9) (1967) 165–173.
[6] V.D. Zhak, V.A. Mukhin, V.E. Nakoryakov, Three-dimensional flow and heat transfer in a rectangular cavity, J. Appl. Mech. Tech. Phys. 22 (2) (1981) 186–189.
[7] J.R. Koseff, R.L. Street, On end wall effects in a lid-driven cavity flow, Trans. ASME, J. Fluids Eng. 106 (4) (1984) 385–389.
[8] M. Hiwada, I. Mabuchi, M. Kumada, Three-dimensional flow and heat transfer in a rectangular cavity, Heat Transfer Jpn. Res. 14 (1) (1985) 75–96.
[9] E.M. Sparrow, D.L. Misterek, Mass transfer at the base of a cylindrical cavity recessed in the floor of a flat duct, Trans. ASME, J. Heat Transfer 108 (4) (1986) 859–866.
[10] K. Greichen, V.I. Kornilov, Some features of a turbulent flow in a square cavity, Preprint No. 11–94, Inst. Theor. Appl. Mech., Sib. Div., Acad. Sci. USSR, Novosibirsk, 1994, pp. 1–31 (in Russian).
[11] A.D. Gosman, E.E. Khalil, J.H. Whitelaw, The calculation of two dimensional turbulent recirculating flows, turbulent shear flows, 1, Springer Verlag, Heidelberg, 1979.
[12] A.A. Khalatov, G.V. Kovalenko, S.G. Kobsar', Modeling of hydrodynamics and heat transfer in an air flow past surfaces with cavities of different shapes, Ind. Heat Eng. 26 (5) (2004) 20–26.
[13] V.I. Terekhov, N.I. Yarygina, A.Yu. D'yachenko, Turbulent heat transfer in a cross flow cavity with inclined sidewalls, Proc. of the 12th Intern. Heat Transfer Conf., Grenoble, France, vol. 2, Paris, Elsevier, 2002, pp. 615–619.
[14] A.Yu. D'yachenko, V.I. Terekhov, N.I. Yarygina, Heat transfer in a crossflow cavity with inclined walls in a turbulized flow, in: Proc. V Minsk Intern. Forum on Heat and Mass Transfer (MMF-V), Minsk, Belarus', May 24–28, 2004. Minsk: Inst. Heat Mass Transfer, CD ROM, pp. 1–29 (in Russian).
[15] V.Yu. Mityakov, Capabilities of bismuth-based gradient heat-flux probes in a thermal engineering experiment, Candidate's Dissertation in Technical Sciences, St. Petersburg, 2005 (in Russian).
[16] H. Yamamoto, N. Seki, S. Fukusako, Forced-convection heat transfer on heated bottom surface of a cavity, Trans. ASME, J. Heat Transfer 101 (3) (1979) 475–479.
[17] R.F. Richards, M.F. Young, J.C. Haiad, Turbulent forced convection heat transfer from a bottom heated open surface cavity, Int. J. Heat Mass Transfer 30 (11) (1987) 2281–2287.
[18] V.I. Terekhov, N.I. Yarygina, Forced-convection heat transfer from the bottom of trenches with rectangular or inclined walls, Exp. Heat Transfer 9 (1996) 133–148.
[19] V.I. Terekhov, N.I. Yarygina, A.Yu. D'yachenko, A.V. Shaporin, Specific features of vortex formation and heat transfer in three-dimensional crossflow cavities, Proceedings of the IV Minsk International Forum on Heat and Mass Transfer (MMF-IV), Minsk, Belarus', May 22–26, vol. 1, Institute Heat Mass Transfer, Minsk, pp. 28–35 (in Russian).
[20] H.C. Kuhlman, M. Wanschura, H.J. Rath, Elliptic instability in two-sided lid-driven cavity flow, Eur. J. Mech. B. Fluids 17 (4) (1998) 561–569.
[21] A.Yu. D'yachenko, V.I. Terekhov, N.I. Yarygina, Turbulent flow past a transverse cavity with inclined side walls. 1. Flow structure, J. Appl. Mech. Tech. Phys. 47 (5) (2006) 671–678.

[22] A.F. Charwat, C.F. Dewey, J.N. Ross, J.A. Hitz, An investigation of separated flows. 2. Flow in the cavity and heat transfer, J. Aerospace Sci. 8 (7) (1961) 513–527.
[23] R.A. Seban, Heat transfer and flow in a shallow rectangular cavity with subsonic turbulent air flow, Int. J. Heat Mass Transfer 8 (1965) 1353–1358.
[24] J. Fox, Heat transfer and air flow in a transverse rectangular ditch, Int. J. Heat Mass Transfer 7 (1965) 269–279.
[25] V.V. Degtyareva, V.A. Mukhin, V.E. Nakoryakov, Experimental study of mass transfer in axisymmetric cavities, J. Eng. Phys. 43 (2) (1982) 181–185.
[26] V.I. Terekhov, N.I. Yarygina, Heat-transfer laws in cavities exposed to a turbulent flow, Ind. Heat Eng. 19 (4/5) (1997) 133–148.
[27] V.I. Terekhov, S.P. Tret'yakov, N.I. Yarygina, Convective heat transfer from the bottom of cavities of different geometries, forced convection of single-phase fluid, Proceedings of the I Russian National Conference on Heat Transfer, Moscow, November 21–25, vol. 1, Moscow Energy Inst., 1994, pp. 256–261 (in Russian).
[28] V.I. Terekhov, N.I. Yarygina, Heat transfer in separation regions of turbulized flows, forced convection of single-phase fluid, Proceedings of the II Russian National Conference on Heat Transfer, Moscow, October 26–30, vol. 2, Moscow Energy Inst., 1998, pp. 244–247 (in Russian).
[29] O.A. Kabov, I.V. Marchuk, V.M. Chupin, Thermal imaging study of the liquid film flowing on vertical surface with local heat source, Russ. J. Eng. Thermophys. 6 (2) (1996) 104–138.
[30] V.I. Terekhov, S.V. Kalinina, Flow and heat transfer in a single spherical cavity: state of the problem and unanswered questions (review), Thermophys. Aeromech. 9 (4) (2002) 475–496.
[31] P.K. Chang, Separation of Flow, Pergamon Press, Oxford, 1970, pp. 770.